Field effect in chalcogenide glasses

Robert C. Frye* and David Adler

*Department of Electrical Engineering and Computer Science
and Center for Materials Science and Engineering,
Massachusetts Institute of Technology, Cambridge, Massachusetts 02139*
(Received 25 November 1980)

It is generally believed that chalcogenide glasses contain large densities of defect centers characterized by a negative effective correlation energy. If so, the Fermi level should be pinned and at most a small field effect should be observed. Nevertheless, there have been several reports of significant field effects in chalcogenide glasses. In this work, we report the results of new field-effect measurements on amorphous $Te_{39}As_{36}Si_{17}Ge_7P_1$. We find that the response is dominated by very slow transients which take several hours to reach steady state at room temperature. The steady-state field effect is consistent with the concept of defects characterized by a negative effective correlation energy, but the transient response is difficult to understand. We show that first-order kinetic model of carrier trapping by valence alternation pairs explains the transient effects observed in a natural way. We also demonstrate that field-effect measurements as a function of time and temperature can be used to evaluate qualitatively both the defect densities and energies. This analysis further enables us to understand apparent inconsistencies in the previously reported results. The defects investigated appear to be characteristic of all Te-As based glasses.

I. INTRODUCTION

There has been a great deal of progress recently in understanding the unique properties of chalcogenide glasses. These materials are characterized by a pinned Fermi energy together with the absence of a significant unpaired spin density. Anderson[1] suggested that these two observations would be compatible if electrons near the Fermi energy possessed a negative effective correlation energy, U_{eff}. Mott et al.[2,3] proposed that this negative U_{eff} characterized electrons localized on defect centers such as chalcogen dangling bonds, and showed how such a model could also be used to understand the photoconductivity and photoluminescence results. Kastner et al.[4] showed how these concepts follow naturally from the particular electronic structure of chalcogen atoms which are capable of forming charged defect centers with a very low creation energy. In a pure chalcogen such as Se, these are positively charged threefold-coordinated atoms $(C_3{}^+)$ and negatively charged, singly-coordinated atoms $(C_1{}^-)$, a combination called a valence alternation pair (VAP). In chalcogenide alloys such as As_2Se_3, other VAP's such as $C_3{}^+$-$P_2{}^-$ pairs are likely.[5] The low creation en-

ergy of such VAP's ensures that there are always large densities frozen in as the material is quenched below the glass transition temperature. The negative effective correlation energy arises because the two different types of defect structures, e.g., C_3 and C_1, have coordination numbers which differ by two. Consequently, a structural transformation involving only a bond breaking or bond formation together with a small atomic relaxation is sufficient to transform from one type of defect to the other.

II. PREDICTED BEHAVIOR OF THE FIELD EFFECT IN AMORPHOUS SEMICONDUCTORS

Field-effect studies of amorphous semiconductors have been a very active area of interest for many years, because they directly probe the localized states in the gap which control the electronic properties of the material. Ordinarily, a thin-film-transistor (TFT) structure such as the one shown in Fig. 1(a) is used. The actual geometry may vary depending on the details of the fabrication process, but the basic elements are common to all. The TFT consists of two parallel source and drain electrodes and a gate electrode which is isolated from

the semiconductor by an insulating layer. The gate, insulator, and semiconductor form a parallel-plate capacitor. When a voltage is applied across this capitator, charges are induced in the semiconductor. The band diagram for a typical bias condition is shown in Fig. 1(b). The charges induced in the semiconductor are not located directly at the semiconductor-insulator interface, but are instead distributed spatially in the bulk of the semiconductor. It is this feature which gives rise to the field effect.

The charge induced in the semiconductor consists of two major components. One component is the immobile trapped charge residing in the defect states. The other is a mobile charge which is induced beyond the conduction- or valence-band mobility edge. In the experiment, a small bias is applied between the source and drain electrodes, and the resulting change in the conductance is measured. The experiment thus observes the change in the mobile-charge component induced by an applied gate voltage V_G.

If the distribution of charge in the semiconductor occurs in a region which is narrow compared to the insulator thickness t_i, then to a good approximation the total induced charge per unit area Q is given by

$$Q = \frac{V_G \epsilon_i}{t_i} , \qquad (1)$$

where ϵ_i is the dielectric permittivity of the insulator. This total charge consists of two components,
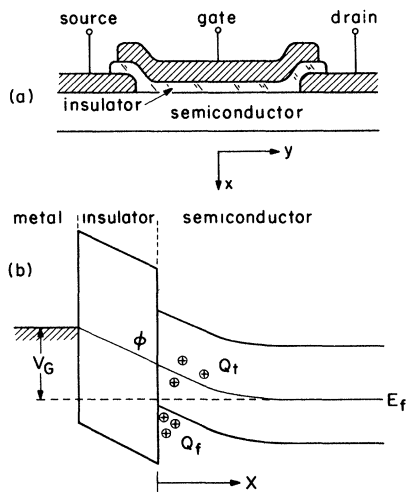

FIG. 1. (a) Cross section of basic thin-film-transistor structure. (b) Typical energy bands versus distance perpendicular to the gate electrode.

$$Q = Q_F + Q_T , \qquad (2)$$

where Q_F is the free charge and Q_T is the trapped charge. If the distance between the source and drain electrodes is L and the width of the conducting path is Z, then the change in conductance ΔG is

$$\Delta G = \mu Q_F \frac{Z}{L} , \qquad (3)$$

where μ is the mobility of the free charge. Thus, for a constant applied source-to-drain voltage V_{DS}, the change in current ΔI can be written as

$$\Delta I = (\Delta G) V_{DS} = \mu Q_F \frac{Z}{L} V_{DS}$$
$$= \left[\frac{\mu Q_F}{Q_F + Q_T} \right] \frac{Z}{L} \frac{\epsilon_i}{t_i} V_{DS} V_G , \qquad (4)$$

where we have used Eqs. (1)–(3). The quantity in parentheses in Eq. (4) is the effective mobility, which is often called the trap-limited mobility. It is this quantity which is measured in field-effect experiments. The dependence of the trap-limited mobility on applied bias and temperature provides information about the nature of the free as well as the trapped charge.

Thus far, we have not made use of the fact that chalcogenide glasses contain defects which are characterized by a negative effective correlation energy. This is important because of the breakdown of ordinary Fermi statistics when electronic correlations cannot be neglected. A careful statistical analysis[6] shows that the average occupancy per defect site $\bar{n}$ for the case of a negative U_{eff} obeys the relation (for $kT << |U_{eff}|$)

$$\bar{n} = \frac{1}{2}[1 + \tanh(E_F - \mu_0)/kT] , \qquad (5)$$

where E_F is the position of the Fermi energy and μ_0 is the average energy to add two electrons to a positively charged defect (thereby converting it to a negatively charged defect).

Equation (5) resembles the behavior of a system that obeys Fermi statistics, but one in which all the defects are located at μ_0. Thus, negatively correlated defects such as VAP's strongly pin the Fermi energy. (Of course, the explanation of the observed strong Fermi-energy pinning is one of the major successes of the VAP model.) We shall subsequently analyze the behavior of $\bar{n}$ in detail. However, the important point to emphasize here is that the Fermi-energy pinning suggested by Eq. (5) should manifest itself in a field-effect experiment by the observation of very small values of Q_F and

hence of ΔI. Consequently, the VAP model predicts that chalcogenide glasses should exhibit, at most, an extremely weak field effect.

III. PREVIOUS FIELD-EFFECT STUDIES OF CHALCOGENIDE GLASSES

The earliest reported attempt to measure the field effect in chalcogenide glasses was by Fritzsche and Ovshinsky,[7] who found no measurable effect and concluded that the density of states at the Fermi energy was larger than 10^{19} cm^{-3}eV^{-1}. Later measurements by Egerton[8] and Levy et al.[9] showed that a step voltage applied to the gate yielded a transient modulation which decayed to an immeasurably small value. Tick and Watson[10] observed a field effect in Te$_2$AsSi, but their results varied widely between samples prepared under identical conditions.

The entire situation was changed when Marshall and Owen[11] obtained reliable results on films of both As$_2$Te$_3$ and As$_{30}$Te$_{48}$Si$_{12}$Ge$_{10}$. These results, shown in Figs. 2 and 3, show enhanced conductance when positive charge is induced into the glasses, indicating the predominance of free-hole transport. Marshall and Owen concluded that the density of states of both glasses had the form sketched in Fig. 4. For negative values of V_G, states are pulled up with respect to E_F, thus inducing positive charge in the defect levels below E_F and in the valence band. In this model, the induced mobile charge is less than the induced trapped charge by a multiple of the appropriate Boltzmann factor, and therefore the trap-limited mobility μ_T is proportional to

$$\mu_T \simeq \mu \frac{Q_F}{Q_T} \propto \exp[-(E_v - E_1)/kT] \ ,$$
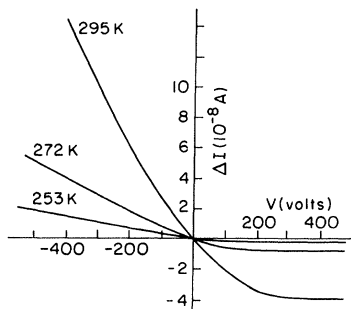
where E_1 is the energy of the trap. This explains

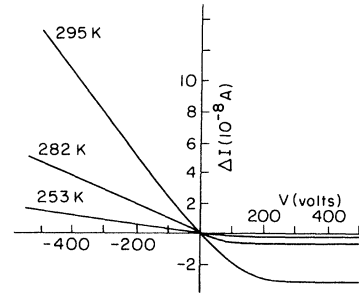FIG. 2. TFT characteristics of As$_2$Te$_3$ (after Marshall and Owen, Ref. 11).

FIG. 3. TFT characteristics of As$_{30}$Te$_{48}$Si$_{12}$Ge$_{10}$ (after Marshall and Owen, Ref. 11).

the observed activated behavior in Figs. 2 and 3. For positive values of V_G the current saturates, suggesting the presence of trapping levels above E_F.

The results of Mahan and Bube[12] showed generally similar behavior at room temperature, but differed from those of Marshall and Owen at higher temperatures. Mahan and Bube suggested that at high temperatures the mobile carriers screen the induced charge efficiently, although this explanation requires a very low hole mobility, about 5×10^{-5} cm^{2}V^{-1}sec^{-1}. Very recently, Radjy and Green[13] found behavior similar to that of Marshall and Owen, but also observed that the field-effect modulation decays to a negligibly small value with time. They proposed that this behavior results from the effects of trapping by localized states in the vicinity of the Fermi energy.

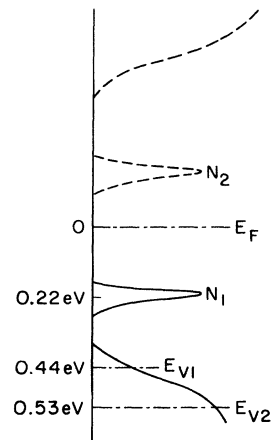From our present point of view, the most impor-

FIG. 4. Proposed density of states for As$_2$Te$_3$ and As$_{30}$Te$_{18}$Si$_{12}$Ge$_{10}$. E_{V1} is the position of valence band edge for As$_{30}$Te$_{18}$Si$_{12}$Ge$_{10}$; E_{V2} is the position of valence band edge for As$_2$Te$_3$. $N_1 = 10^{19} - 10^{20}$ cm^3. N_2 is of suitable energy and density to fix E_f at the position indicated (after Marshall and Owen, Ref. 11).

tant point is not the origin of the time dependence or even the temperature dependence of the field effect, but rather why the field effect is measurable at all. If chalcogenide glasses necessarily possess large densities of negatively correlated defects, then the analysis given in Sec. II indicates that the field-effect response should be negligibly small, and this prediction is in apparent disagreement with all of the recently reported results.[11−13] It is the purpose of this paper to report new experimental results on the field effect of a multicomponent chalcogenide glass (Sec. IV), analyze in great detail the steady-state reponse which would be expected from our current understanding of this class of materials, quantitatively confirming the discrepancy between theory and experiment (Sec. V), analyze the *transient* field effect (Sec. VI), and thereby resolve the apparent dilemma in a natural way, without the introduction of any new types of defect or other *ad hoc* assumptions.

IV. FIELD-EFFECT CHARACTERISTICS OF AMORPHOUS $Te_{39}As_{36}Si_{17}Ge_7P_1$

In order to investigate the field effect in chalcogenide glasses experimentally, we chose a multicomponent alloy $Te_{39}As_{36}Si_{17}Ge_7P_1$, which had previously been intensively studied at both low and high fields.[14] A cross section of the basic device structure is shown in Fig. 5. The devices were fabricated by first thermally oxidizing a heavily doped crystalline silicon substrate to form a layer of SiO_2 approximately 5000 Å thick. These samples were subsequently given a very light phosphorus diffusion to convert the upper surface to a phospho-silicate glass to retard dielectric breakdown and to prevent subsequent sodium contamination. Mo source-drain electrodes were then sputter deposited and patterned to form an interdi-
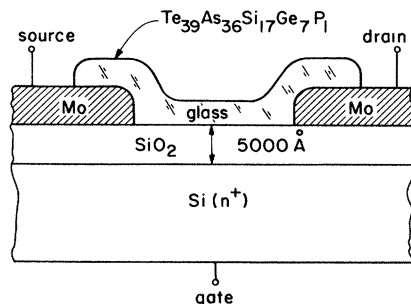
gitated structure with a channel length of 160 μm and a channel width of 9 mm to give a width-to-length ratio of ∼50. Glass films 2000 Å thick were sputter deposited at 15 mTorr pressure in pure Ar after sputter etching to ensure a clean interface. This particular method has several advantages. Thermally grown SiO_2 provides a very reliable thin insulator and avoids many of the leakage and contamination problems encountered with deposited insulators. Since the glass is deposited as the last step in the process, we can avoid subjecting it to any subsequent heating. It is also advantageous to have the glass at the top of the structure because this allows optical measurements to be made on the same device. In the initial stages of the investigation, it was unclear whether or not passivation of the top surface of the glass would be necessary. As it turned out, measurement of the characteristics in a dry nitrogen ambient eliminated undesired effects from this top layer.

To obtain the field-effect modulation, the source was biased at 10 V and the resulting drain current was monitored using a Keithley 610C electrometer. Measurements made in air proved to be unreliable, probably because of leakage. However, with the dry nitrogen ambient, currents could be reliably measured down to pA levels. For our measurements, two gate-voltage wave forms were used, shown in Fig. 6. To obtain the drain current as a function of gate voltage, a linear ramp with variable period P was used. Time-varying gate voltages couple to the drain through the gate-to-drain capacitance and, therefore, give rise to an undesired current signal. By using a linear ramp, this current is a constant which changes sign depending on whether the gate voltage is increasing or decreasing. This constant current can be easily identified in the final data and subtracted out. For transient decay measurements, a simple gate-voltage step was used.

Figure 7 shows the experimental bulk drain
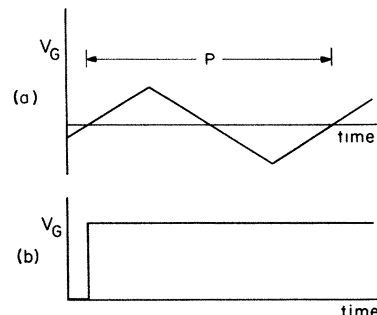
FIG. 5. TFT device structure used in this work.
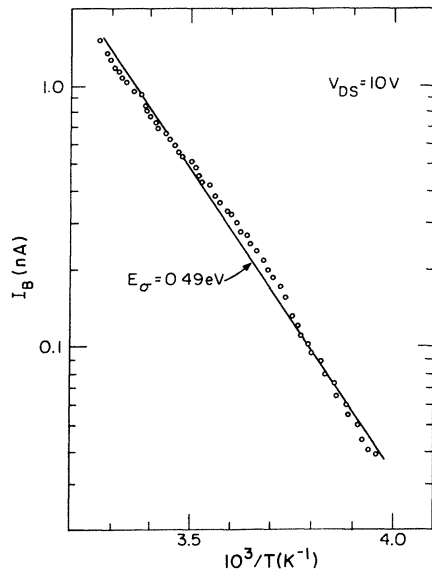
FIG. 6. Gate-voltage wave forms.

FIG. 7. Bulk current versus temperature for the conditions described in the text.

current as a function of temperature with the gate at zero and the source at 10 V. These results correspond to a room-temperature conductivity of 10^{-7} Ω^{-1}cm^{-1} and show a well-defined activation energy of 0.49 eV, both in excellent agreement with previous results.[14] The fact that these results match those obtained on sandwich structures indicates that we do not have significant carrier accumulation or depletion occuring at either the semiconductor-insulator interface or at the top surface of our glass.

The form of a typical I_D versus V_G measurement is shown in Fig. 8. For a ramp period of 1 min, considerable hysteresis occurs. To facilitate presentation and analysis of the data, we shall subse-
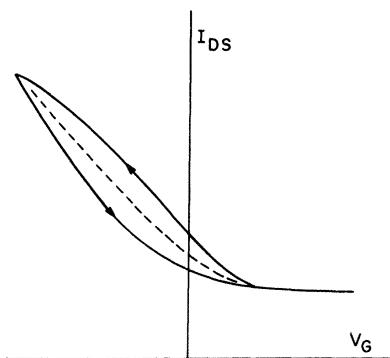
quently indicate the average current as shown by the dashed line. The hysteresis was most pronounced at low temperatures and high sweep rates, as expected in a strongly trapped system.

Figure 9 shows the total drain current as a function of gate voltage at several temperatures for a sweep period of 1 min. In Fig. 10 we show the same results with the zero gate-voltage current subtracted out. These results are very similar to those of Marshall and Owen,[11] which were obtained in a comparable time. When we vary the sweep period at room temperature, we obtain the data shown in Fig. 11. These results closely resemble those of Radjy and Green.[13] The astonishing feature is that in our case the field effect persists for times on the order of hours, whereas theirs decays in a few seconds. This result provides a clue as to the reason why field effects are sometimes seen at "dc" and sometimes not. It would appear that the time to reach equilibrium can be extremely long in some materials. We find that the field effect continues to decay, tending toward an immeasurably small value for times up to 10 h.

Figure 12 shows the result of a transient decay experiment at room temperature. The gate voltage was switched from zero to a negative voltage, at which point the field-effect modulation is large. For both 20- and 40-V pulses, the behavior is the same. After a relatively fast initial decay, the

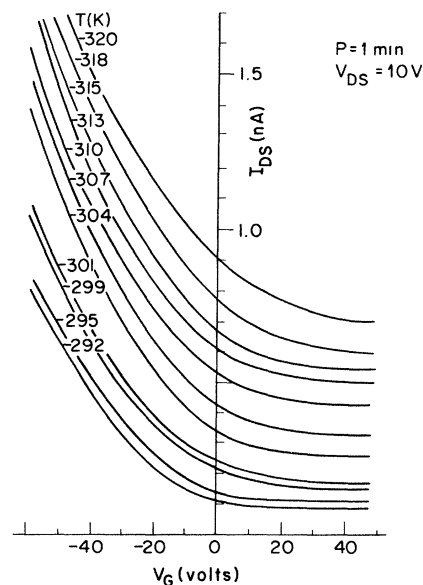FIG. 8. Typical source-to-drain current versus gate voltage.

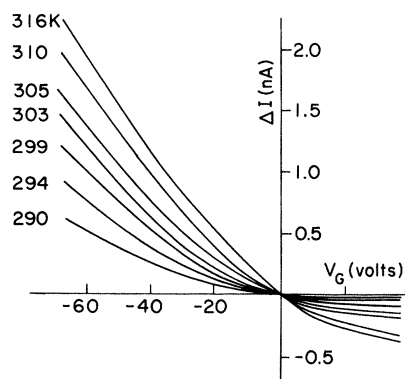FIG. 9. Total source-to-drain current versus gate voltage at various temperatures.

FIG. 10. Change in source-to-drain current versus gate voltage at various temperatures.

FIG. 12. Transient decay of the field-effect current.

current shows a long time decay constant of about 130 min. We shall defer a more detailed examination of the temperature behavior of this decay until the next section.

This result, together with the results of Radjy and Green[13] suggests that *all* field-effect results previously reported in these materials are transient. Furthermore, the similarity of our results at short times to those of Marshall and Owen[11] indicates that we are measuring the same basic process that they observed, particularly since it is difficult to identify the slower decay after the fast initial transient. In view of all of the field-effect results thus far reported on chalcogenide glasses, it appears reasonable to conclude that the ability to observe the effect is a function of the time constant rather than of the trap density.

V. ANALYSIS OF THE EQUILIBRIUM FIELD EFFECT IN CHALCOGENIDE GLASSES

Since the characteristics of thin-film transistors depend critically on the nature of the defect states
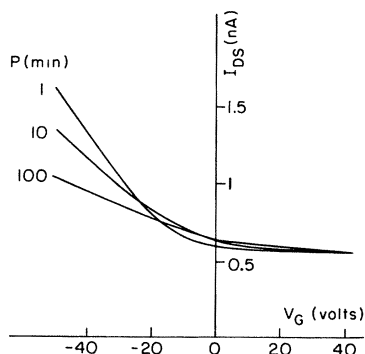

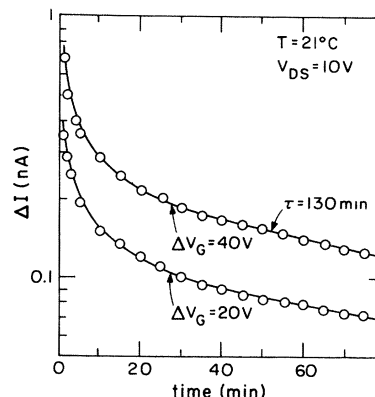FIG. 11. Room-temperature source-to-drain current versus gate voltage for various sweep periods.

in the gap, it is vital to analyze these states very carefully. This is especially true when the predominant defects are characterized by a negative effective correlation energy, as is expected to be the case in chalcogenide glasses. In this section we first discuss the nature of the major defects in amorphous As-Te alloys and analyze their behavior at equilibrium. We shall then consider the kinetics of the transient field effect.

A. Defects in amorphous As-Te alloys

For simplicity, let us first consider a stoichiometric alloy such as As_2Te_3. In the ideal network, each As atom bonds to three neighboring Te atoms. This situation is sketched in Fig. 13(a). Departures from stoichiometry and material inhomogeneities will alter this picture to some degree, but we will take this as our prototypical ideal glass. Local geometry constraints and thermodynamic considerations imposed by material preparation can give rise to a variety of bonding defects within this ideal framework.[15,16] However, we would expect that one type of defect would have the lowest creation energy and thus dominate. For As_2Te_3, a VAP such as $C_3^+-P_2^-$ is most likely the predominant defect.[16] (We are using the notation of Kastner et al.[4] in which C denotes a chalcogen center, P a pnictide center, the subscript the coordination number, and the subscript the charge state.) A threefold-coordinated Te atom is sketched in Fig. 13(b) and a twofold-coordinated As atom is sketched in Fig. 13(c). It is clear that the latter can be created from the former by a simple bond breaking and relaxation. This is one of the requirements for a negative U_{eff}. The other is that the reaction
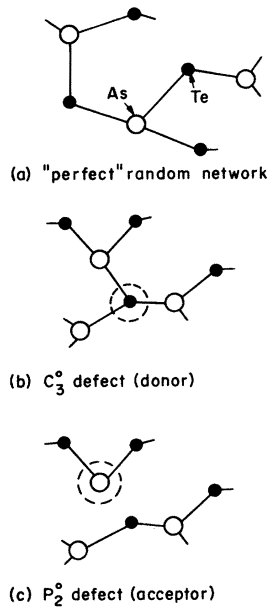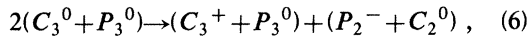
(a) "perfect" random network

(b) C_3^0 defect (donor)

(c) P_2^0 defect (acceptor)

FIG. 13. Possible bonding configurations in As_2Te_3.

$$2(C_3^0 + P_3^0) \rightarrow (C_3^+ + P_3^0) + (P_2^- + C_2^0) , \quad (6)$$

is exothermic. But since C_3^+ and P_2^- are optimally bonded centers for their electronic configurations, it is reasonable to expect that (6) is indeed exothermic. Thus a C_3^+-P_2^- pair acts like a VAP, and has the properties discussed by Kastner et al.[4,17] The C_3^0 center acts like a donor while the P_2^0 center acts like an acceptor. Because the two neutral centers involve different atoms, it is not clear which has the lower energy, but this is unimportant for our general discussion. [The particular form used in (6) assumes that C_3^0 has lower energy than P_2^0, but the term on the left could just as well be $2(C_2^0 + P_2^0)$.] In fact, the neutral defect is better envisioned as a defective bond which could be centered on either the chalcogen (as an overcoordination) or the pnictide (as a dangling bond).

Note that a P_4^+-C_1^- VAP is also possible and is likely to have a negative effective correlation energy. Since P_4 centers require an s-p promotion, we feel that this VAP probably has a larger

creation energy than a C_3^+-P_2^- pair.[16] However, even if this is not the case, the analysis presented in this section remains applicable provided only that one particular type of VAP predominates.

B. Generalized statistics of negatively correlated defects

We shall assume that our chalcogenide glass is characterized by three major features: (1) a valence band with an effective density of states N_V, (2) a conduction band with an effective density of states N_c, and (3) a density N of VAP's. We further assume that the effects of other gap states are negligible and that band tailing is not important. Actually, this later assumption is not too stringent because we can generally include the effects of narrow band tails by simply redefining the mobility to account for the fraction of immobile carriers below the mobility edges.

Since the detailed nature of the VAP's is not critical, we shall simply recognize that one center is donorlike and the other acceptorlike. Thus, we consider that a single defect can exist in one of four states,

$$d^+, d^0, a^0, a^- .$$

The state d^+ is that of an unoccupied defect ($n = 0$), and can be taken to be the zero of energy. Let T_0 be the energy of the neutral donor and $T_0 + W$ be the energy of the neutral acceptor. These are the two possible configurations for the singly occupied defect ($n = 1$), and both are doubley degenerate because of two spin possibilities. If the acceptor is the lower-energy neutral defect, W is negative. Finally, the negatively, charged acceptor represents the doubly occupied defect ($n = 2$) and it has energy $2T_0 - U$, where U is the magnitude of the negative effective correlation energy. Then, the grand partition function is given by

$$Z = 1 + 2(e^{-(T_0 - \mu)/kT} + e^{-(T_0 + W - \mu)/kT})$$
$$+ e^{-(2T_0 - U - 2\mu)/kT} . \quad (7)$$

and the average occupation by

$$\bar{n} = kT \frac{\partial}{\partial \mu}(\ln Z) = \frac{2[(e^{-(T_0 - \mu)/kT} + e^{-(T_0 + W - \mu)/kT}) + e^{-(2T_0 - U - 2\mu)/kT}]}{Z} . \quad (8)$$

At equilibrium $\bar{n} = 1$, and Eq. (8) shows that the

Fermi energy is simply

$$\mu_0 = T_0 - \frac{U}{2} . \qquad (9)$$

Since we are interested in deriving an expression

for the field effect, we must consider the consequences of an applied electrostatic potential ϕ. Then, the electrochemical potential becomes

$$\mu = E_F - q\phi \qquad (10)$$

and the average charge ρ_T is given by

$$\rho_T = N(\bar{n} - 1) = \frac{N(e^{-(E_F - \mu_0 - q\phi)/kT} + e^{(E_F - \mu_0 - q\phi)/kT})}{e^{-(E_F - \mu_0 - q\phi)/kT} + 2(e^{-U/2kT} + e^{-(U/2 + W)/kT}) + e^{(E_F - \mu_0 - q\phi)/kT}} . \qquad (11)$$

For $U \gg 2kT$ and $(W + U/2) \gg kT$, Eq. (11) becomes

$$\rho_T = N \tanh[(E_F - \mu_0 - q\phi)/kT] , \qquad (12)$$

where we have taken $\rho_T = 0$ when $\phi = 0$ and $E_F = \mu_0$. However, since there can be some charge in the valence and conduction bands, we must modify this condition. The charge in the conduction band is

$$\rho_n = -N_c \exp[-(E_c - E_F)/kT] ,$$

while that in the valence band is

$$\rho_p = N_v \exp[-(E_F - E_v)/kT] .$$

Thus, E_F is determined from the relation

$$N \tanh[(E_F - \mu_0)/kT] + N_v e^{-(E_F - E_v)/kT}$$
$$- N_c e^{-(E_c - E_F)/kT} = 0 . \qquad (13)$$

Generally, N is of the order of 10^{19} cm^3, whereas at room temperature ρ_n and ρ_p are only of the order of 10^{10} cm^3. Thus, to a very good approximation $E_F = \mu_0$, i.e., the position of the Fermi level is determined by the VAP's at equilibrium.

However, we have not yet taken into account the important fact that the donors and acceptors can interconvert by either the breaking or the formation of a bond. In order to analyze this, we note that the density of ionized donors is given by

$$N_D^+ = N_D \frac{1}{1 + 2e^{-(T_0 - \mu)/kT}} ,$$

while the density of ionized acceptors is

$$N_A^- = N_A \frac{1}{1 + 2e^{[T_0 - (W + U) - \mu]/kT}} .$$

For $\phi = 0$, we can use Eq. (9) for μ to obtain

$$N_D^+ = N_D \frac{1}{1 + 2e^{-(U/2 - E_F)/kT}} \qquad (14)$$

and

$$N_A^- = N_A 1 + 2e^{-(U/2 + W - E_F)/kT} . \qquad (15)$$

As expected, N_D donor states are at an energy $U/2$ above the equilibrium Fermi energy and N_A acceptors are at an energy $W + U/2$ below the equilibrium Fermi energy. In addition, we must have

$$N_D = N_A = N . \qquad (16)$$

Because of the possibility of interconversion of the neutral donors and acceptors, at equilibrium we can write

$$N_D^0 = e^{W/kT} N_A^0 . \qquad (17)$$

This leads to the relationships

$$N_D \simeq \frac{N}{2} \{1 + \tanh[(E_F - q\phi)/kT]\} \qquad (18)$$

and

$$N_A \simeq \frac{N}{2} \{1 - \tanh[(E_F - q\phi)/kT]\} . \qquad (19)$$

Thus, the densities of donor and acceptor states vary with applied electrostatic potential. This is the effect that gives rise to the strong pinning of the Fermi energy in chalcogenide glasses. The process is sketched in Fig. 14. At equilibrium, the donor and acceptor densities are equal, as indicated in Fig. 14(a). If the Fermi energy is increased by a process such as an applied potential or electron injection, the initial effect is to neutralize some of the ionized donor states and ionize some of the neutral acceptor states, as shown in Fig. 14(b). But this leads to an imbalance in Eq. (17), so that neutral donors begin to convert to neutral acceptors and eventually ionized acceptors. As the acceptor density increases, the Fermi energy is pulled back down to very near its original position, as indicated in Fig. 14(c).

This result has several important consequences. Consider the behavior of the charge as given in Eq. (12). This function can be interpreted in terms of conventional Fermi statistics, indicating that the charge responds to application of a potential as if
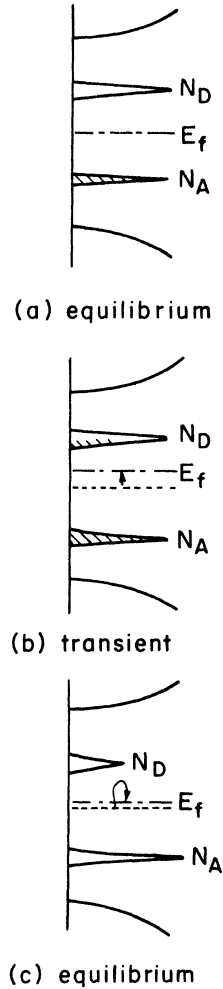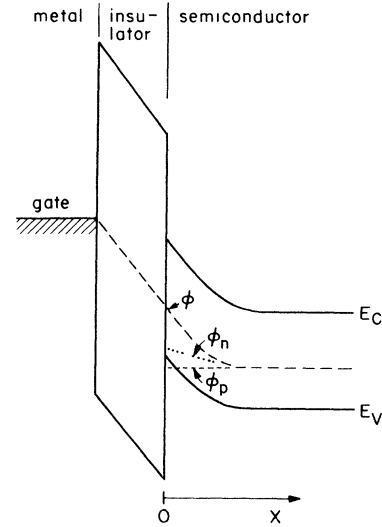
(a) equilibrium

(b) transient

(c) equilibrium

FIG. 14. Fermi-energy pinning by VAP's.

FIG. 15. Energy bands versus distance for MIS structure; ϕ_n and ϕ_p are the electron and hole quasi-Fermi levels, respectively.

C. Equilibrium field-effect characteristics

We shall now derive the field-effect characteristics at equilibrium. Figure 15 shows the behavior

there were a large density of one-electron states at the Fermi energy. However, as is clear from Fig. 14(a), in reality there are *no* one-electron states at E_F. This is reflected in the donor and acceptor occupation relations, Eqs. (14) and (15). Thus, the overall behavior of the charge does not obey the same statistics as the donor and acceptor levels. This is a key point that is generally disregarded in the analysis of the field effect in materials containing negatively correlated defects. The relative densities of donors and acceptors are not independent but depend sensitively on the potential.

of the bands for a metal-insulator—semiconductor (MIS) structure. Since no current can flow across the insulator, we can immediately write down Poisson's equation in the semiconductor as

$$\nabla^2\phi = \frac{q}{\epsilon_s}[-N\tanh\beta\phi + p_0(e^{-\beta\phi}-1)$$

$$-n_0(e^{\beta\phi}-1)] , \qquad (20)$$

where ϵ_s is the dielectric susceptibility, p_0 and n_0 the equilibrium bulk concentration of holes and electrons, and $\beta = q/kT$. We want to solve this equation subject to the boundary conditions imposed by the applied gate voltage. We ignore the metal-to-semiconductor work-function difference and the effects of trapped charge at the interface. Since we are dealing with p-type materials, we neglect the contribution of free electrons to the last term of Eq. (20). Thus, we must solve

$$\frac{d^2\phi}{dx^2} = \frac{q}{\epsilon_s}[-N\tanh\beta\phi + p_0(e^{-\beta\phi}-1)] .$$

$$(21)$$

We solve Eq. (21) in Appendix A. For small surface potential, the field-effect current is [Eq. (A6)]

$$\Delta I_{DS} = \pm\left[\mu_p\frac{p_0}{p_0+N}\right]V_{DS}V_G\frac{\epsilon_i}{t_i}\frac{Z}{L} \qquad (22)$$

so that the trap-limited mobility is given by

$$\mu_T = \mu_p \frac{p_0}{p_0 + N} \quad . \tag{23}$$

Note that since p_0 is activated, the trap-limited mobility will be activated for $N \gg p_0$, and will, furthermore, show the same activation as the bulk conductivity. An activated mobility is a major characteristic of a trap-limited conduction process.

When typical values are inserted for the parameters, $N \sim 10^{19}$ cm^{-3} and $V_G/t_i \sim 10^6$ V/cm, Eq. (A5) indicates that the small $\beta\phi_s$ approximation is valid and thus Eq. (22) applies. However, the experimental results discussed in Sec. III are in complete disagreement with this prediction with regard to not only the shape and magnitude of the field-effect current but also its temperature behavior. In all reported measurements, the field-effect mobility has a much lower activation energy than does the bulk conductivity. Figure 16 compares the predictions of Eq. (22) with the experimental results[11,12] at room temperature. It is clear that the theory is in much better agreement with studies that fail to detect any field-effect modulation at all.[7,9]

Note also that the density of states inferred by Marshall and Owen[11] shown in Fig. 4 is very similar to the predicted density of states sketched in Fig. 14(a); however, Marshall and Owen do not observe the effects of interconversion of donors and acceptors. A similar conclusion follows from the low-temperature results of Mahan and Bube[12] and the short-time results of Radjy and Green.[13] If all of the previously reported results are to be consistent with the same basic behavior, we must reconcile the facts that (1) in some cases, no field effect is detectable, (2) stable dc field effects have been observed and are consistent with the density
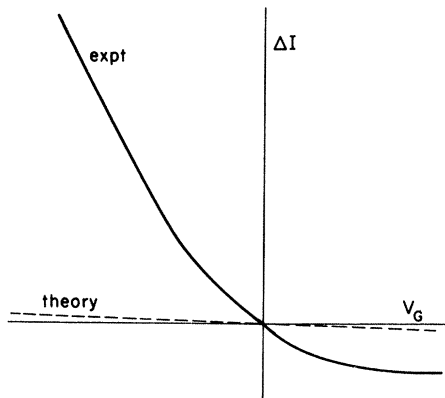
of states sketched in Fig. 14(a), (3) unstable field effects have been observed which initially are consistent with the stable results but which decay to a very small value, and (4) stable dc results have been obtained which change their behavior at high temperatures. We shall show in the next section that a careful analysis of the effects of time and temperature on the measurements indeed can reconcile all these results.

VI. ANALYSIS OF TRANSIENT FIELD EFFECT IN CHALCOGENIDE GLASSES

In our model a defect can exist in any one of four states, and transitions between these occur via charge transfer and/or atomic relaxations. The situation is simplified, however, since not all states are connected by a single-step process. Rather, the transitions occur via the sequence

$$N_D^+ \leftrightarrow N_D^0 \leftrightarrow N_A^0 \leftrightarrow N_A^- \quad .$$
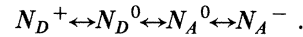
This means that we need not consider processes such as, for example, $N_A^- \leftrightarrow N_D^0$, since this cannot occur in a single step. The rates that describe the above transitions fall into two categories, viz., carrier exchange between traps and the valence or conduction band and configurational changes. We shall neglect direct charge transfer from trap to trap. The transitions are illustrated in Fig. 17. Let us consider first the charge-transfer rates. We can analyze these rates in the same manner as trap-assisted recombination in crystalline semiconductors.[18,19] Consider, for example, the reaction,

$$N_D^+ + n \leftrightarrow N_D^0 \quad .$$
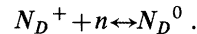
This reaction involves capture of a free electron by

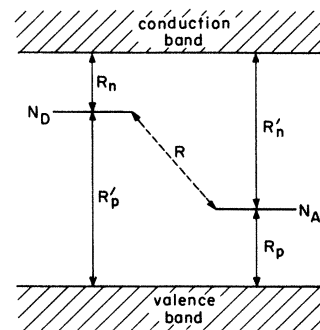FIG. 16. Experimental and theoretical TFT characteristics.

FIG. 17. Schematic illustration of single-step transitions. Solid lines indicate charge transfer from donors (N_D) and acceptors (N_A) to the conduction and valence band. Dashed line indicates configurational changes.

a positively charged donor and the inverse process of emission of an electron by a neutral donor. This rate can be written as

$$R_n = C_n N_D{}^0 - N_D{}^+ n s_n v_T \ , \tag{24}$$

where n is the free-electron density, n_T is the thermal velocity of the electron, and s_n is the capture cross section. The product $s_n v_T$ represents the capture volume swept out by the carrier per unit time. By the principle of detailed balance, this rate must be identically zero at thermal equilibrium. From our previous analysis, Eqs. (14)—(19), at equilibrium,

$$N_D{}^0 = 2e^{-U/2kT} N_D{}^+$$

$$\equiv \alpha_D N_D{}^+ \tag{25}$$

and

$$n = n_0 \ .$$

Substituting these relations into Eq. (24) with $R_n = 0$, we obtain C_n. The final result is

$$R_n = \frac{N_D{}^0}{\alpha_D} n_0 s_n v_T - N_D{}^+ n s_n v_T \ . \tag{26}$$

In cases where the mean free path of a free carrier becomes small compared to the capture radius, it is more appropriate in the above equation to use the carrier diffusion velocity rather than the thermal velocity.[20] To circumvent this problem, we shall use a phenomenological relaxation time τ_n defined by

$$\frac{1}{\tau_n} \equiv n_0 s_n v_n \ , \tag{27}$$

where v_n is the appropriate velocity. We then obtain

$$R_n = \frac{1}{\tau_n} \left[\frac{N_D{}^0}{\alpha_D} - N_D{}^+ + \frac{n}{n_0} \right] \ . \tag{28}$$

In an entirely analogous manner, the rate for the process

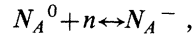$$N_A{}^- + p \leftrightarrow N_A{}^0$$
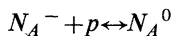
can be written

$$R_p = \frac{1}{\tau_p} \left[\frac{N_A{}^0}{\alpha_A} - N_A{}^- \frac{p}{p_0} \right] \ , \tag{29}$$

where $\alpha_A \equiv 2 \exp[-(W + U/2)kT]$ and $\tau_p{}^{-1} = p_0 s_p v_p$.

The two remaining charge-transfer rates are similar, except that they now involve the capture of

free electrons and holes by *neutral* centers. We shall denote the capture cross sections for these processes by s_n' and s_p', respectively. We then find that for the process
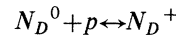
$$N_A{}^0 + n \leftrightarrow N_A{}^- \ ,$$

we obtain

$$R_n' = \frac{1}{\tau_n'} \left[\alpha_A N_A{}^- - N_A{}^0 \frac{n}{n_0} \right] \ , \tag{30}$$

where

$$\frac{1}{\tau_n'} = n_0 s_n' v_n' \ .$$

Similarly, for the process

$$N_D{}^0 + p \leftrightarrow N_D{}^+$$

we obtain

$$R_p' = \frac{1}{\tau_p'} \left[\alpha_D N_D{}^+ - N_D \frac{p}{p_0} \right] \tag{31}$$

where

$$\frac{1}{\tau_p'} = p_0 s_p' v_p' \ .$$

In the rates given by Eqs. (28)—(31), it is important to keep in mind the distinction between charged and neutral capture centers. Generally, the capture cross section for a charged defect is expected to be several orders of magnitude larger than that for a neutral defect. Since the other parameters, viz., the equilibrium free-carrier concentrations and velocities are comparable for all four processes, we can safely assume that

$$\frac{1}{\tau_n}, \frac{1}{\tau_p} \gg \frac{1}{\tau_n'}, \frac{1}{\tau_p'} \ .$$

In order to keep this distinction clear, in the remainder of the analysis all neutral capture processes will be indicated by primed variables.

The remaining rate to consider is that of configurational change, i.e., the rate at which donors become acceptors and vice versa. This change most likely occurs only when the defects are neutral; i.e., a reaction such as

$$N_A{}^- \rightarrow N_D{}^-$$
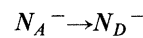
is extremely unlikely to occur. Tight-binding estimates[4] indicate that the final state in such a process is a very high-energy defect and is not statistically favored. We need only, therefore, consider the reaction

$$N_A{}^0 \leftrightarrow N_A{}^0 .$$

In this process, the neutral acceptor is at an energy W above the neutral donor. We can write the corresponding rate to first order from mass-action considerations as

$$R = \frac{1}{\tau}(N_A{}^0 - e^{-W/kT} N_D{}^0)$$

$$= \frac{1}{\tau} \left[N_A{}^0 - \frac{\alpha_A}{\alpha_D} N_D{}^0 \right] , \tag{32}$$

where τ is the relaxation time. For a simple tran-

sition between these two states, we might expect τ to be of the order of a phonon time, but for the present we shall not make any assumptions about its magnitude. It is important to recognize that W may be negative in which case

$$R = \frac{1}{\tau} \left[\frac{\alpha_D}{\alpha_A} N_A{}^0 - N_D{}^0 \right] .$$

This possibility, however, can simply be incorporated into our definition of τ. Using Eqs. (29)—(32), we can write the total rates of change of the defects as

$$\frac{d}{dt} N_D{}^+ = \frac{1}{\tau_n} \left[\frac{N_D{}^0}{\alpha_D} - N_D{}^+ \frac{n}{n_0} \right] - \frac{1}{\tau_p'} \left[\alpha_D N_D{}^+ - N_D \frac{p}{p_0} \right] , \tag{33}$$

$$\frac{d}{dt} N_A{}^- = \frac{1}{\tau_p} \left[\frac{N_A{}^0}{\alpha_A} - N_A{}^- \frac{p}{p_0} \right] - \frac{1}{\tau_n'} \left[\alpha_A N_A{}^- - N_A{}^0 \frac{n}{n_0} \right] , \tag{34}$$

and

$$\frac{d}{dt}(N_D{}^0 + N_D{}^+) = -\frac{d}{dt}(N_A{}^0 + N_A{}^-)$$

$$= \frac{1}{\tau} \left[N_A{}^0 - \frac{\alpha_A}{\alpha_D} N_D{}^0 \right] . \tag{35}$$

The first equality in (35) results from the requirement that the total number of defects is conserved, i.e.,

$$N_D{}^0 + N_D{}^+ + N_A{}^0 + N_A{}^- = N . \tag{36}$$

Thus, we have four independent equations. In addition, we must also consider the rate of change of the free carriers:

$$\frac{dp}{dt} = \frac{1}{\tau_p} \left[\frac{N_A{}^0}{\alpha_A} - N_A{}^- \frac{p}{p_0} \right]$$

$$+ \frac{1}{\tau_p'} \left[\alpha_D N_D{}^+ - N_D{}^0 \frac{p}{p_0} \right] - \frac{1}{q} \nabla J_p \tag{37}$$

and

$$\frac{dn}{dt} = \frac{1}{\tau_p} \left[\frac{D^0}{\alpha_D} - N_D{}^+ \frac{n}{n_0} \right]$$

$$+ \frac{1}{\tau_n'} \left[\alpha_A N_A{}^- - N_A{}^0 \frac{n}{n_0} \right] + \frac{1}{q} \nabla J_n , \tag{38}$$

where J_p and J_n are the hole and electron current

densities. Equations (33)—(35) relate the change in defect populations to changes in the free-carrier densities. It is more convenient for the purposes of the field-effect analysis to express them, instead, in terms of the potential. We do this by introducing the electron and hole quasi-Fermi levels, ϕ_n and ϕ_p, which are defined by the relationships

$$n = n_0 e^{\beta(\phi - \phi_n)}$$

and

$$p = p_0 e^{-\beta(\phi - \phi_p)} .$$

Equations (33)—(36) then become

$$\frac{d}{dt} N_D{}^+ = \frac{1}{\tau_n} \left[\frac{N_D{}^0}{\alpha_D} - N_D{}^+ e^{\beta(\phi - \phi_n)} \right]$$

$$- \frac{1}{\tau_p'} (\alpha_D N_D{}^+ - N_D{}^0 e^{-\beta(\phi - \phi_p)}) , \tag{39}$$

$$\frac{d}{dt} N_A{}^- = \frac{1}{\tau_p} \left[\frac{N_A{}^0}{\alpha_A} - N_A{}^- e^{-\beta(\phi - \phi_n)} \right]$$

$$- \frac{1}{\tau_n'} (\alpha_A N_A{}^- - N_A{}^0 e^{\beta(\phi - \phi_p)}) , \tag{40}$$

and

$$\frac{d}{dt}(N_D{}^0 + N_D{}^+) = -\frac{d}{dt}(N_A{}^0 + N_A{}^-)$$

$$= \frac{1}{\tau} \left[N_A{}^0 - \frac{\alpha_A}{\alpha_D} N_D{}^0 \right] . \tag{41}$$

Let us examine, for a moment, the two remaining rates, Eqs. (37) and (38). The final term in both equations represents the change in the free-carrier density which arises from charging currents in the bulk. The current densities in these terms are proportional to the gradients of the respective quasi-Fermi levels. The terms force the quasi-Fermi levels for both carrier types to zero within the dielectric relaxation time

$$\tau_D^{-1} \simeq \sigma_B / \epsilon_s \; ,$$

where σ_B is the bulk conductivity. From our previous measurements, we calculate this time to be 10^{-5} sec [taking the dielectric constant ϵ_s equal to 9 (Ref. 13)]. Thus, on a time scale of minutes it is clearly safe to assume that $\phi_n = \phi_p = 0$. For the purposes of the field-effect analysis, we start with the six basic equations:

$$\frac{d}{dt} N_D^+ = \frac{1}{\tau_n} \left[\frac{N_D^0}{\alpha_D} - N_D^+ e^{\beta\phi} \right]$$

$$- \frac{1}{\tau_p'} (\alpha_D N_D^+ - N_D^0 e^{-\beta\phi}) \; , \qquad (42)$$

$$\frac{d}{dt} N_A^- = \frac{1}{\tau_p} \left[\frac{N_A^0}{\alpha_A} - N_A^- e^{-\beta\phi} \right]$$

$$- \frac{1}{\tau_n'} (\alpha_A N_A^- - N_A^0 e^{\beta\phi}) \; , \qquad (43)$$

$$\frac{d}{dt} (N_D^0 + N_D^+) = - \frac{d}{dt} (N_A^0 + N_A^-)$$

$$= \frac{1}{\tau} \left[N_A^0 - \frac{\alpha_A}{\alpha_D} N_D^0 \right] \; , \qquad (44)$$

$$N_D^0 + N_D^+ + N_A^0 + N_A^- = N_T \; , \qquad (45)$$

$$p = p_0 e^{-\beta\phi} \; , \qquad (46)$$

$$n = n_0 e^{\beta\phi} \; . \qquad (47)$$

The time-dependent Poisson's equation now follows from Eqs. (42)—(47). We can rewrite Eqs. (42) and (43) as

$$\frac{d}{dt} N_D^+ - (N_D^0 - \alpha_D N_D^+ e^{\beta\phi}) \left[\frac{1}{\alpha_D \tau_n} + \frac{e^{-\beta\phi}}{\tau_p'} \right]$$

$$\qquad\qquad\qquad\qquad\qquad\qquad\qquad (48)$$

and

$$\frac{d}{dt} N_A^- = (N_A^0 - \alpha_A N_A^- e^{-\beta\phi}) \left[\frac{1}{\alpha_A \tau_p} + \frac{e^{\beta\phi}}{\tau_n'} \right] \; .$$

$$\qquad\qquad\qquad\qquad\qquad\qquad\qquad (49)$$

As discussed previously, $\tau_n \ll \tau_p'$ and $\tau_p \ll \tau_n'$. In addition, both α_D and α_A are small by definition. Thus, the lifetimes appearing in the last terms of Eqs. (48) and (49) are independent of ϕ provided the bands are not bent sufficiently that the Fermi energy reaches the donor or acceptor levels

$$-(W + U/2) \ll q\phi \ll U/2 \; .$$

If this is the case, Boltzmann statistics are applicable, and Eqs. (42)—(44) become

$$\frac{d}{dt} N_D^+ = (N_D^0 - \alpha_D N_D^+ e^{\beta\phi}) \frac{1}{\alpha_D \tau_D} \; , \qquad (50)$$

$$\frac{d}{dt} N_A^- = (N_A^0 - \alpha_A N_A^- e^{-\beta\phi}) \frac{1}{\alpha_A \tau_p} \; , \qquad (51)$$

and

$$\frac{d}{dt} (N_D^0 + N_D^+) = - \frac{d}{dt} (N_A^0 + N_A^-)$$

$$= \left[N_A^0 - \frac{\alpha_A}{\alpha_D} N_D^0 \right] \frac{1}{\tau} \; . \qquad (52)$$

In each of the above rate equations, the expression in parentheses is comparable, being of the order of a neutral trap density. Thus, the relative magnitudes of the three time constants τ, $\alpha_A \tau_p$, and $\alpha_D \tau_n$ are critical. The value of any one of these may vary over a range of several orders of magnitude, and at different temperatures any one of them could be very small or very large compared to the others. It would, in fact, require very special circumstances for two of these time constants to be comparable. Charge transfer occurs by a three-step process. For example, when negative charge is trapped, the process is

$$N_D^+ \to N_D^0 \to N_A^0 \to N_A^- \; .$$
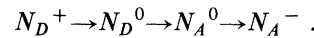
In this three-step process, it is reasonable to assume that the overall transfer rate $N_D^+ \to N_A^-$ is controlled by the *slowest step*. We shall solve Eqs. (50)—(52) by assuming that the two fast rates quasistatically follow the slow changes arising from the third rate.

It is important to identify which one of the three steps is the rate-limiting one. If we use typical values for the capture cross section and velocity of the carriers to estimate τ_n and τ_p, we find that these are much too small to explain the very slow transient response that we observe. Consequently, only τ, which results from the configurational change, can be sufficently large, and Eq. (52) represents the rate-limiting process. Because $\alpha_D \tau_n$ and $\alpha_A \tau_p$ are small compared to τ, a small imbal-

ance in the two terms on the right of Eq. (50) or (51) leads to a very large rate of change of $N_D{}^+$ or $N_A{}^-$, thus restoring the balance. Therefore, we must solve the set of approximate equations

$$\frac{d}{dt}N_D{}^+\simeq 0=(N_D{}^0-\alpha_D N_D{}^+ e^{\beta\phi})\frac{1}{\alpha_D\tau_n} , \quad (53)$$

$$\frac{d}{dt}N_A{}^-\simeq 0=(N_A{}^0-\alpha_A N_A{}^- e^{-\beta\phi})\frac{1}{\alpha_A\tau_p} , \quad (54)$$

and

$$\frac{d}{dt}(N_D{}^0+N_D{}^+)=-\frac{d}{dt}(N_A{}^0+N_A{}^-)$$

$$=\left[N_A{}^0-\frac{\alpha_A}{\alpha_D}N_D{}^0\right]\frac{1}{\tau} . \quad (55)$$

We can rewrite Eq. (55) as

$$\frac{d}{dt}\left[\rho_T+\frac{(\alpha_D e^{\beta\phi})-\alpha_A e^{-\beta\phi})N+\rho_T(\alpha_D e^{\beta\phi}+\alpha_A e^{-\beta\phi}+2\alpha_A\alpha_D)}{\alpha_A e^{-\beta\phi}+\alpha_D e^{\beta\phi}+2}\right]$$

$$=\frac{2\alpha_A}{\tau}\left[\frac{N(e^{-\beta\phi}-e^{\beta\phi})-\rho_T(e^{-\beta\phi}+e^{\beta\phi}+\alpha_A+\alpha_D)}{\alpha_A e^{-\beta\phi}+\alpha_D e^{\beta\phi}+2}\right] . \quad (57)$$

In the Boltzmann limit, Eq. (57) becomes

$$\frac{d}{dt}(\rho_T+N/2(\alpha_D e^{\beta\phi}-\alpha_A e^{-\beta\phi}))$$

$$=\frac{2\alpha_A\cosh\beta\phi}{\tau}(-N\tanh\beta\phi-\rho_T) . \quad (58)$$

Equation (58) is the basic relation between the trapped charge and perturbations in the potential. If the system is initially at rest with $\rho_T=0$ and $\phi=0$, and we perturb ϕ for a time $0<t<<\tau$, the time integral of the right-hand side of Eq. (58) is negligible, and

$$\rho_T(t=0^+)=\frac{N}{2}(\alpha_D e^{\beta\phi}-\alpha_A e^{-\beta\phi})+K ,$$

where K is a constant determined by the trapped charge when $\phi=0$. In the present case,

$$K=-\frac{N}{2}(\alpha_D-\alpha_A) .$$

K can be incorporated inside the time derivative in Eq. (58), resulting in

$$\frac{d}{dt}[\rho_T+\tfrac{1}{2}\alpha_D N(e^{\beta\phi}-1)-\tfrac{1}{2}\alpha_A N(e^{-\beta\phi}-1)]$$

$$=\frac{2\alpha_A\cosh\beta\phi}{\tau}(-N\tanh\beta\phi-\rho_T) . \quad (59)$$

$$\frac{d}{dt}(N_D{}^+-N_A{}^-)+(N_D{}^0-N_A{}^0))$$

$$=\frac{d}{dt}(\rho_T-(N_D{}^0-N_A{}^0))=\left[N_A{}^0-\frac{\alpha_A}{\alpha_D}N_D{}^0\right]\frac{2}{\tau} , \quad (56)$$

where ρ_T is the trapped charge density.
   Conservation of defects requires

$$N_A{}^0\left[1+\frac{e^{\beta\phi}}{\alpha_A}\right]+N_D{}^0\left[1+\frac{e^{-\beta\phi}}{\alpha_D}\right]=N$$

and

$$\rho_T=N_D{}^0\frac{e^{-\beta\phi}}{\alpha_D}-N_A{}^0\frac{e^{\beta\phi}}{\alpha_A} .$$

Solving these two equations for $N_A{}^0$ and $N_D{}^0$ and substituting into Eq. (56), we find

Equation (59) is of the form

$$\frac{d}{dt}[\rho_T-\rho_0(\phi)]=\nu(\phi)[\rho_e(\phi)-\rho_T] ,$$

where $\nu(\phi)$ is an appropriate frequency, $\rho_0(\phi)$ is the initial (high-frequency) response, and $\rho_e(\phi)$ is the equilibrium (steady-state) response. In the steady state,

$$\rho_T=\rho_e(\phi)=-N\tanh\beta\phi ,$$

the same result obtained from the statistical analysis of the last section [see Eq. (12)]. However, for times small compared to τ,

$$\rho_T=\rho_0(\phi)=\tfrac{1}{2}\alpha_A N(e^{-\beta\phi}-1)-\tfrac{1}{2}\alpha_D N(e^{\beta\phi}-1) .$$

In the Boltzmann limit, this is the trapped charge density that arises from $N/2$ acceptors located at an energy $W+U/2$ below the equilibrium Fermi energy and $N/2$ donors located at an energy $U/2$ above E_F. This is consistent with our short-time results as well as those of Radjy and Green,[13] and is also in agreement with the data of Marshall and Owen.[11] But more important, Eq. (59) explains the unusual decay of the field effect with time observed by Radjy and Green[13] and by us.
   It is important to evaluate the response at intermediate times, in order to analyze the observed de-

cay curves. This is carried out in Appendix B. We find that the initial decay is given by Eq. (B24),

$$\frac{d}{dt}(\Delta I) + \frac{2}{\tau}\Delta I \simeq 0 \ , \tag{60}$$

so that the field effect initially decays with a time constant of $\tau/2$. However, at later times, the solution is given by Eq. (B25):

$$\frac{d}{dt}\Delta I + \left[\frac{4\alpha_A}{(\alpha_A + \alpha_D)\tau}\right]I \simeq 0 \ , \tag{61}$$

so that for large times and small currents, the rate of decay is

$$\frac{\tau}{2}\left[\frac{\alpha_A + \alpha_D}{2\alpha_A}\right] \ .$$

For $W > 0$, $\alpha_D \gg \alpha_A$, so that the final rate of decay is actually much slower. This behavior is illustrated in Fig. 18. The asymptotic behavior is in good agreement with the experimental results shown in Fig. 12.

Let us briefly consider the reason for this dual time-constant behavior. The limiting rate is given by Eq. (35):

$$\frac{d}{dt}(N_D) = -\frac{d}{dt}(N_A) = \frac{1}{\tau}\left[N_A{}^0 - \frac{\alpha_A}{\alpha_D}N_D{}^0\right] \ .$$

The sequence of events in a transient experiment is indicated in Fig. 19. Initially, free holes flood the space-charge region and are trapped very quickly by the negatively charged acceptors. This causes $N_A{}^0$ to be too large, and the excess neutral acceptors decay with a time constant τ (the factor of 2 enters because we have effectively made a transition from $N_A{}^-$ to $N_D{}^+$, capturing two holes). This process, in turn, leads to an increase in the charge density and a corresponding decrease in the screen-
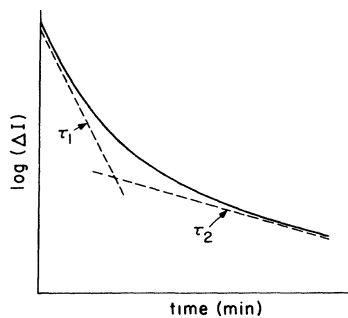
ing length. This means that holes trapped deep in the bulk must be reemitted and moved nearer to the surface. The process occurs as a sequence of two events. As the potential collapses, some donors give up their holes, leading to excess $N_D{}^0$; these decay with a time constant $\tau\alpha_D/\alpha_A$. The resulting neutral acceptors quickly give up another hole to become negatively charged. The two holes emitted in this overall process then move to the surface and become trapped, again converting acceptors to donors. The overall rate for the sum of two processes is given by

$$\frac{1}{\tau} = \frac{(1/\tau)(\alpha_A/\alpha_D\tau)}{(1/\tau)+(\alpha_A/\alpha_D\tau)} = \frac{1}{\tau}\frac{\alpha_A}{\alpha_A + \alpha_D} \ .$$

(We find two factors of 2 that must enter into the above rate. One factor enters because the overall process involves two carriers as before, the other because for very small values of ϕ we begin to get an additional equal contribution from electrons as well as holes.)

Our results suggest that W can be determined from field-effect experiments. According to the model τ_1, the short-time decay rate, is related to τ_2, the long-time decay rate, by the simple relationship

$$\tau_1 = \frac{2\alpha_A}{\alpha_A + \alpha_D}\tau_2 \simeq \frac{2\alpha_A}{\alpha_D}\tau_2 = 2e^{-W/kT}\tau_2 \ . \tag{62}$$
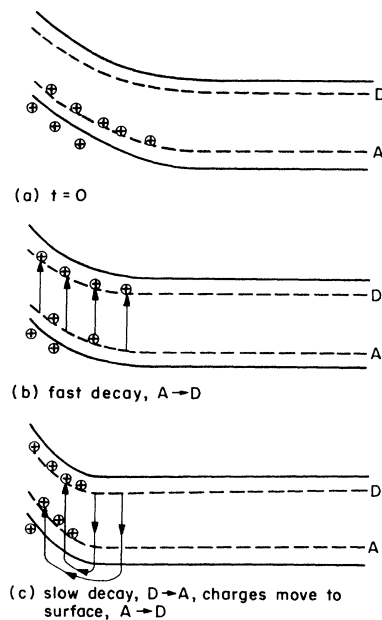
FIG. 18. Asymptotic behavior of field-effect current transient decay.

(a) t = 0

(b) fast decay, A→D

(c) slow decay, D→A, charges move to surface, A→D

FIG. 19. Sequence of events for transient decay experiment.

Thus, we can obtain W from the ratio of τ_1 and τ_2.

In Fig. 20 we show the results of transient decay measurements at various temperatures. The table in the inset shows the time constants and the inferred values of W. The values can be seen to give a consistent result over the entire temperature range. In addition, these data give us an explanation for the high-temperature anomalies observed by Mahan and Bube.[12] This is because the curves extrapolate to a value such that the $t = 0$ current always increases with increasing temperature. At $t = 20$ min, however, this behavior is completely reversed. Depending on the time scale of the measurement, it is possible to be led to the conclusion either that the field-effect current increases or decreases with increasing temperature. The physical origin of this is the fact that at higher temperatures the transient current decays at a much faster rate. This effect is illustrated dramatically by a plot of the transconductance in the high-current region as a function of temperature, shown in Fig. 21. From the short-term analysis we expect this to behave as

$$\frac{d}{dV_G}(\Delta I) = g_m = \left[\frac{\mu p_0}{p_0 + (\alpha_A N/2)} \right] \frac{Z}{L} V_{DS} \frac{\epsilon_i}{t_i}$$

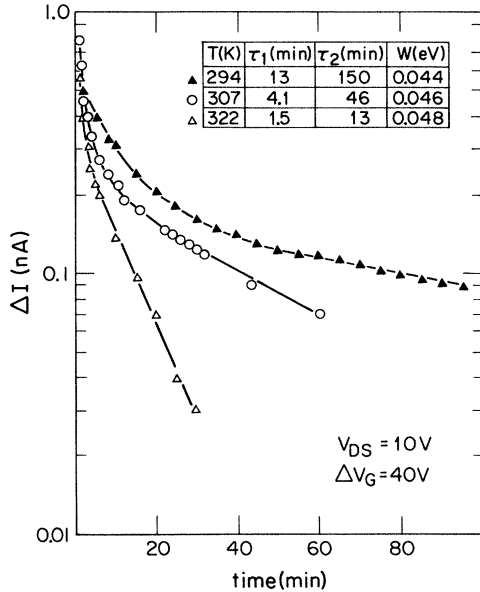$$\propto e^{-(E_\sigma - U/2 - W)/kT} ,$$

$$(63)$$

where E_σ is the activation energy of the bulk conductivity (p_0). The data fit an activated curve quite well at low temperature, but g_m begins to fall off dramatically at high temperature. This is because field-effect current decays significantly within the 1-min time in which it is measured. This clearly demonstrates the need to account for time-constant effects carefully when choosing a particular measurement procedure.

From the activation energy of the transconductance, we can conclude that $(U/2) - W = 0.25 \pm 0.05$ eV. Furthermore, we have found $W = 0.043 + 00.02$ eV. We can, therefore, completely determine the effective density of states in the gap of our films. The transconductance is given by

$$g_m = \left[\frac{\mu_p p_0}{p_0 + (\alpha_A N/2)} \right] \frac{Z}{L} V_{DS} \frac{\epsilon_i}{t_i}$$

and the bulk dark current is

$$I_B = q \mu_p p_0 \frac{Z}{L} V_{DS} d .$$

For $\alpha_A N/2 \gg p_0$, the ratio of I_B to g_m is

$$\frac{I_B}{g_m} \simeq q \left[\frac{\alpha_A N}{2} \right] \frac{t_i d}{\epsilon_i} .$$

Thus, N can be evaluated as

$$N = \frac{2\epsilon_i I_B}{g_m t_i d \alpha_A} \simeq 10^{20} \text{ cm}^3 .$$

Note that the above expression is independent of either the mobility or the free-carrier density, and is expressed entirely in terms of measurable quantities. However, it is quite sensitive to errors in determining the values of the energies U and W

T(K)	τ_1(min)	τ_2(min)	W(eV)
▲ 294	13	150	0.044
○ 307	4.1	46	0.046
△ 322	1.5	13	0.048

$V_{DS} = 10$ V
$\Delta V_G = 40$ V

FIG. 20. Transient current decay at various temperatures. Table shows values of asymptotic time constants and inferred value of W.
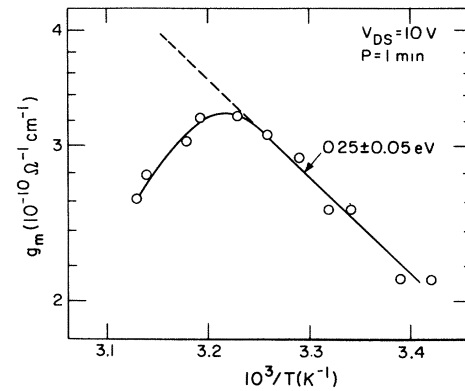

FIG. 21. Transconductance in the high-current region versus temperature.

which enter into α_A. The effective density of states derived from our analysis is shown in Fig. 22. It is important to bear in mind that the indicated equal densities of ionized donors and acceptors applies only to the equilibrium situation. Any shift in the Fermi energy produces net concentration changes.

Let us consider the details of the acceptor-to-donor transition. We still have not explained the origin of the unusually long time constant that we observe. The situation becomes clearer if we plot τ_1 and τ_2 versus temperature. This is shown in Fig. 23. Clearly, both τ_1 and τ_2 are activated. This leads us to conclude that τ itself is activated. Thus, the transition from acceptor to donor and back appears to require thermal assistance in either direction. This suggests the existence of some kind of energy barrier between the two states, as indicated in the energy-configuration diagram Fig. 24. Acceptors decay with a rate given by

$$\frac{1}{\tau} = (2 \times 10^8)e^{-0.65/kT}\,\text{sec}^{-1} \ .$$

The attempt-to-escape frequency of 2×20^8 sec^{-1} is somewhat low, but this extrapolated value is extremely sensitive to errors in the activation energy and leads us to suspect that within our experimental error the higher values of activation are probably more realistic.

The analysis presented here provides a straightforward explanation of not only our own data, but also the large variations in experimental field-effect behavior that have been reported. Nearly all of the successful measurements have been made using glasses containing a relatively high percentage of As and Te. As is clear from our transient analysis, the ability to observe a measurable field effect depends critically on the time constants for carrier
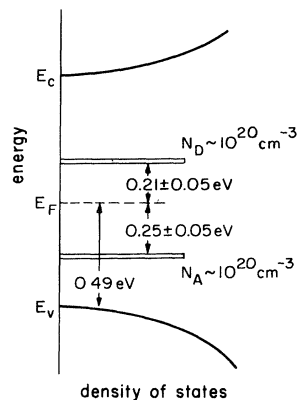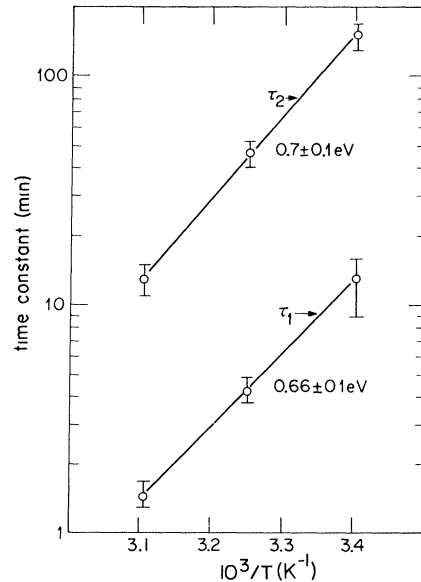

FIG. 23. Initial decay time constant τ_1 and final decay time constant τ_2 versus temperature.

trapping. These two facts strongly indicate that the long time-constant behavior is very closely associated with As and Te. It also lends considerable support to our previous suggestion of the existence of a predominant VAP in these materials. For other chalcogenide glasses such as selenides, we would certainly expect a difference in the activation energy of the acceptor-to-donor transition. But even a small change in the energy barrier can cause orders-of-magnitude difference in the time constant. This may account for the inability to observe field-effect modulation in such materials as As_2Se_3 and Se. Our analysis suggests that it may be possible to measure a field effect in these materials provided that the frequency is sufficiently high. However, the trapping kinetics may then involve time constants which are smaller than the dielec-

FIG. 22. Effective one-electron density of states at equilibrium obtained from transient analysis.
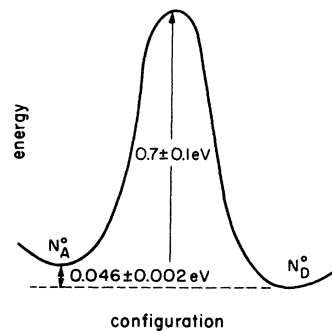

FIG. 24. Energy-configuration diagram for the neutral acceptor-to-donor transition.

tric relaxation time, in which case the field effect would effectively be damped out.

An important conclusion of our study is that the neutral donor has lower total energy than the neutral acceptor. If the predominant VAP is a $C_3{}^+$-$P_2{}^-$ pair, then we can conclude that the energy of the $C_3{}^0$ center is lower than that of the $P_2{}^0$ center. On the other hand, if the predominant VAP is a $P_4{}^+$-$C_1{}^-$ pair, then the $P_4{}^0$ center has lower energy than the $C_1{}^0$. In any event, the existence of two neutral defects is consistent with the observation of two EPR signals at low temperatures in optically excited amorphous arsenic chalcogenides[21] and with the analysis of recent switching experiments[22] involving the same composition used in the present work.

are populated upon the trapping of excess free carriers. The activation energies determined from field-effect decay curves can be used to evaluate both the energies of the defect centers and the density of VAP's. The model explains the previously puzzling wide dispersion of field-effect results reported in chalcogenide glasses. In particular, it also suggests that the failure to observe a field effect to date in Se-based glasses is due to very short time constants for the decay. Most important of all, the analysis emphasizes the dangers of interpreting the electronic structure of a system containing states with a negative U_{eff} in terms of a conventional one-electron density-of-states diagram. If this is done, it must be recognized that the effective density of states can change drastically with *time*.

VII. CONCLUSIONS

We have shown that the steady-state field effect for a material with a significant density of defects characterized by a negative effective correlation energy should be extremely small. If a field-effect response is observed, it is just a transient which should decay away with increasing time. We have associated this transient with the existence of a potential barrier between the two neutral centers that

APPENDIX A: CALCULATION OF THE EQUILIBRIUM FIELD EFFECT

In this appendix we solve Eq. (21) for the field-effect characteristics at equilibrium. Multiplying both sides of Eq. (21) by $2d\phi/dx$ and integrating, we obtain

$$\left[\frac{d\phi}{dx}\right]^2 \Bigg|_{x=\infty}^{x=0} = -\int_{\phi=0}^{\phi=\phi_s} 2\frac{q}{\epsilon_s}[-N\tanh\beta\phi + p_0(e^{-\beta\phi}-1)]d\phi$$

$$= \frac{2q^2N}{\epsilon_s kT}\left[\ln\cosh\beta\phi + \frac{p_0}{N}(e^{-\beta\phi}+\beta\phi)\right]_{\phi=0}^{\phi=\phi_s},$$

where ϕ_s is the surface potential. Since the electric field at $x=\infty$ must be zero, we find

$$\left[\frac{d\phi}{dx}\right]_{x=0} = \pm\frac{2}{\beta\lambda_T}\left[\ln\cosh\beta\phi_s + \frac{p_0}{N}(e^{-\beta\phi_s}+\beta\phi_s-1)\right]^{1/2}, \tag{A1}$$

where

$$\lambda_T \equiv \left[\frac{\epsilon_s kT}{q^2N}\right]^{1/2}. \tag{A2}$$

Ordinarily $p_0 \ll N$, and the second term on the right in Eq. (20) is also negligible. λ_T is the screening length arising from the trapped charge. The gate voltage is then given by

$$V_G = \phi_s + \frac{t_i}{\epsilon_i} \epsilon_s \left[\frac{d\phi}{dx}\right]_{x=0} = \phi_s \pm \frac{t_i}{\epsilon_i} \frac{\epsilon_s}{\beta} \frac{2}{\lambda_T} \left[\ln \cosh\beta\phi_s + \frac{p_0}{N_T}(e^{-\beta\phi_s} + \beta\phi_s - 1)\right]^{1/2}, \qquad \text{(A3)}$$

where t_i is the insulator thickness and ϵ_i is the dielectric permittivity of the insulator. The sign of the $\pm$ in Eq. (A3) is just the sign of ϕ_s.

We must now relate the gate voltage to the source-drain current. We shall assume that the source-drain voltage V_{DS}, is small. For a device having channel length L and width Z and for a hole mobility μ_p, the change in current density is

$$\Delta J_p = q\mu_p \frac{V_{DS}}{L} Z\rho_p(x) \ .$$

Integrating, we obtain

$$\Delta I_{DS} = q\mu_p \frac{Z}{L} V_{DS} \int_{x=0}^{\infty} \rho_p(x)dx = q\mu_p \frac{Z}{L} V_{DS} \int_{\phi=\phi_s}^{\phi=0} \frac{\rho_p(\phi)}{d\phi/dx} d\phi$$

$$= \pm q\mu_p \frac{Z}{L} V_{DS} \int_{\phi=\phi_s}^{\phi=0} \frac{p_0(e^{-\beta\phi} - 1)d\phi}{(2/\beta\lambda_T)[\ln\cosh\beta\phi + (p_0/N)(e^{-\beta\phi} + \beta\phi - 1)]^{1/2}}, \qquad \text{(A4)}$$

where the sign takes on the same value as the gate voltage. Equation (A4) can be integrated numerically to give the change in source-drain current as a function of the surface potential, and this together with Eq. (A1) relates the current to the gate voltage. It is important to recognize that there will be an additional background current arising from bulk conduction in the semiconductor, which is

$$I_B = q\mu_p \frac{Z}{L} V_{DS} p_0 d \ ,$$

where d is the semiconductor thickness.

It is instructive to examine Eqs. (A1) and (A4) in the limit of small $\beta\phi_s$. We can then approximate them as

$$V_G \simeq \phi_s + \frac{t_i}{\epsilon_i} \epsilon_s \frac{2}{\lambda_T} \left[1 + \frac{p_0}{N}\right]^{1/2} \phi_s$$

$$\simeq \frac{2\epsilon_s}{\epsilon_i} \frac{t_i}{\lambda_T} \left[1 + \frac{p_0}{N}\right]^{1/2} \phi_s \ , \qquad \text{(A5)}$$

for $t_i \gg \lambda_T$, and

$$\Delta I_{DS} \simeq \pm q\mu_p \frac{Z}{L} V_{DS} \int_{\phi=\phi_s}^{\phi=0} \frac{p_0\beta\phi}{\frac{2}{\lambda_T}(1 + p_0/N)^{1/2}} \frac{d\phi}{\phi}$$

$$= \pm q\mu_p \frac{Z}{L} V_{DS} \frac{p_0\lambda_T\beta\phi_s}{2(1 + p_0/N)^{1/2}}$$

$$\pm \left[\mu_p \frac{p_0}{p_0 + N}\right] V_{DS} V_G \frac{\epsilon_i}{t_i} \frac{Z}{L} \ . \qquad \text{(A6)}$$

Equation (A6) is identical to Eq. (4), with the trap-limited mobility given by

$$\mu_T = \mu_p \frac{p_0}{p_0 + N} \ . \qquad \text{(A7)}$$

APPENDIX B: CALCULATION OF THE TRANSIENT FIELD EFFECT AT INTERMEDIATE TIMES

In this appendix, we solve for the field-effect response at intermediate times. In order to do this,

some simplifying approximations are essential. We shall begin with a linear analysis, which is relatively straightforward and will enable us to understand the physical processes involved. With the insights resulting from this solution, we shall be able to approximate the real situation.

The rate of charge trapping is given by

$$\frac{d}{dt}\left[\rho_T + \frac{\alpha_D N}{2}(e^{\beta\phi}-1) - \frac{\alpha_A N}{2}(e^{-\beta\phi}-1)\right]$$
$$= \frac{2\alpha_A \cosh\beta\phi}{\tau}(-N\tanh\beta\phi - \rho_T) . \quad \text{(B1)}$$

For small $\beta\phi$, Eq. (B1) becomes

$$\frac{d}{dt}\left[\rho_T + \beta\phi\left[\frac{\alpha_D N}{2} + \frac{\alpha_A N}{2}\right]\right]$$
$$= \frac{2\alpha_A}{\tau}(-N\beta\phi - \rho_T) . \quad \text{(B2)}$$

Taking the Laplace transform of Eq. (B2), we find

$$\hat{\rho}_T\left[s + \frac{2\alpha_A}{\tau}\right] = -\beta\hat{\phi}\left[\left[\frac{\alpha_D N}{2} + \frac{\alpha_A N}{2}\right]s + \frac{2\alpha_A N}{\tau}\right]$$

or

$$\hat{\rho}_T = -\frac{\beta\hat{\phi}\left[\left[\frac{\alpha_D N}{2} + \frac{\alpha_A N}{2}\right]s + \frac{2\alpha_A}{\tau}\right]}{\left[s + \frac{2\alpha_A}{\tau}\right]} , \quad \text{(B3)}$$

where $\hat{\rho}_T$ and $\hat{\phi}$ are the Laplace transforms of ρ_T and ϕ. In addition, we have the free charge density

$$\rho_F = p_0(e^{-\beta\phi}-1) ,$$

which yields

$$\hat{\rho}_F \simeq -p_0\beta\hat{\phi} . \quad \text{(B4)}$$

Taking the transform of Poisson's equation, we find

$$\nabla^2\hat{\phi} = \frac{q}{\epsilon_s}(\hat{\rho}_F + \hat{\rho}_T)$$
$$= -\frac{q}{\epsilon_s}\beta\hat{\phi}\frac{\left\{p_0 + N\left[\left[\frac{\alpha_D}{2} + \frac{\alpha_A}{2}\right]s + \frac{2\alpha_A}{\tau}\right]\right\}}{\left[s + \frac{2\alpha_A}{\tau}\right]} . \quad \text{(B5)}$$

We can simplify Eq. (B5) by introducing several new parameters, the free-carrier screening length

$$\frac{1}{\lambda_F^2} \equiv \frac{q^2 p_0}{\epsilon_s kT} ,$$

that $t=0$ trapped-charge screening length

$$\frac{1}{\lambda_{T0}^2} \equiv \frac{q^2 N}{\epsilon_s kT}\left[\frac{\alpha_D}{2} + \frac{\alpha_A}{2}\right] ,$$

and the equilibrium trapped-charge screening length

$$\frac{1}{\lambda_{Te}^2} \equiv \frac{q^2 N}{\epsilon_s kT} .$$

Note that in most cases $\lambda_F \gg \lambda_{T0}$ and λ_{Te}.

With these definitions, Eq. (B5) becomes

$$\nabla^2\hat{\phi} = -\hat{\phi}\frac{\left[\frac{1}{\lambda_F^2} + \left[\frac{s}{\lambda_{T0}^2} + \frac{2\alpha_A}{\tau}\frac{1}{\lambda_{Te}^2}\right]\right]}{s + \frac{2\alpha_A}{\tau}} . \quad \text{(B6)}$$

Furthermore, we shall define the frequency-dependent screening length λ by

$$\frac{1}{\lambda^2(s)} \equiv \frac{\frac{1}{\lambda_F^2} + \left[\frac{s}{\lambda_{T0}^2} + \frac{2\alpha_A}{\tau}\frac{1}{\lambda_{Te}^2}\right]}{s + \frac{2\alpha_A}{\tau}} .$$

Poisson's equation is then simply given by

$$\nabla^2\hat{\phi} = -\frac{\hat{\phi}}{\lambda^2(s)} , \quad \text{(B7)}$$

which has the simple solution

$$\hat{\phi}(x,s) = \hat{\phi}(0,s)e^{-x/\lambda(s)} . \quad \text{(B8)}$$

The boundary condition for $t_i \gg \lambda(s)$ is

$$\frac{d\hat{\phi}}{dx}(x=0,s) \simeq \frac{\hat{V}_G \epsilon_i}{\epsilon_s t_i} = \frac{\hat{\phi}(0,s)}{\lambda(s)} ,$$

so that

$$\hat{\phi}(x,s) = \frac{\hat{V}_G \epsilon_i}{\epsilon_s t_i}\lambda(s)e^{-x/\lambda(s)} . \quad \text{(B9)}$$

Unfortunately, we cannot obtain an analytical form for the inverse transform of Eq. (B9). However, we can evaluate the field-effect characteristics,

$$\Delta\hat{I} = -q\mu\frac{Z}{L}V_{DS}\int p_0\beta\hat{\phi}\,dx$$
$$= -q\mu\frac{Z}{L}V_{DS}\hat{V}_G\frac{\epsilon_i}{\epsilon_i t_i}\beta p_0\lambda^2(s)$$
$$= -\left[\mu\frac{\lambda^2(s)}{\lambda^2}\right]\frac{Z}{L}V_{DS}\frac{\epsilon_i}{t_i}\hat{V}_G . \quad \text{(B10)}$$

Consider, for example, the field-effect response to an applied step voltage on the gate. In this case $\hat{V}_G = \Delta V_G/s$. Taking the inverse transform of Eq. (B10) we find

$$\Delta I(t) = -\mu \frac{Z}{L} V_{DS} \frac{\epsilon_i}{t_i} \Delta V_G \left\{ \frac{\lambda_{T0}^2}{\lambda_F^2} \exp\left[-\frac{2\alpha_A}{\tau} \frac{\lambda_{T0}^2 t}{\lambda_{Te}^2} \right] + \frac{\lambda_{Te}}{\lambda_F^2} \left[1 - \exp\left[-\frac{2\alpha_A}{\tau} \frac{\lambda_{T0}^2 t}{\lambda_{Te}^2} \right] \right] \right\} . \tag{B11}$$

Equation (B11) describes a simple decaying exponential with a time constant given by

$$\tau_{\text{decay}} = \frac{\tau}{2\alpha_A} \frac{\lambda_{Te}^2}{\lambda_{T0}^2} = \frac{\tau(\alpha_A + \alpha_D)}{4\alpha_A} . \tag{B12}$$

Experimentally, we observe an exponentially decaying field-effect mobility. It is clear from the above analysis that this is a very real effect. As more and more free carriers become trapped, the ratio of free to trapped charges decreases. The decay of both the field-effect mobility and the screening length arise from the same fundamental process of charge trapping, and are really two equivalent manifestations of a single kind of behavior.

The observed decay, shown in Fig. 12, is actually not a simple exponential, reflecting a deficiency of the linear analysis. However, using the physical insight obtained from the linearization, we can approximate the real situation. Integrating Eq. (59) directly, we obtain

$$\frac{d}{dt} \int_0^\infty \left[\rho_T + \frac{\alpha_D N}{2} (e^{\beta\phi} - 1) - \frac{\alpha_A N}{2} (e^{-\beta\phi} - 1) \right] dx = \int_0^\infty \frac{2\alpha_A}{\tau} \cosh\beta\phi(-N\tanh\beta\phi - \rho_T) dx . \tag{B13}$$

But Poisson's equation shows

$$\int_0^\infty \rho_T dx + \int_0^\infty \rho_0 (e^{-\beta\phi} - 1) dx = -\frac{\epsilon_i}{\epsilon_s q} \frac{V_G}{t_i} , \tag{B14}$$

and since the field-effect current is

$$\Delta I = q\mu \frac{Z}{L} V_{DS} \int_0^\infty \rho_0 (e^{-\beta\phi} - 1) dx , \tag{B15}$$

we can write

$$\int_0^\infty \rho_0 (e^{-\beta\phi} - 1) dx = \frac{\Delta I}{q\mu \frac{Z}{L} V_{DS}} . \tag{B16}$$

Defining

$$I_0 \equiv q\mu \frac{Z}{L} V_{DS} \rho_0 t_i , \tag{B17}$$

we find

$$\int_0^\infty \rho_T dx = -\frac{\epsilon_i V_G}{t_i q} - \frac{\Delta I}{I_0} t_i . \tag{B18}$$

and

$$\int_0^\infty (e^{-\beta\phi} - 1) dx = \frac{\Delta I}{I_0} t_i . $$

Equation (B13) then becomes

$$\frac{d}{dt} \left[-\frac{\epsilon_i V_G}{t_i q} - \frac{\Delta I}{I_0} \left[\rho_0 + \frac{\alpha_A N}{2} \right] t_i + \frac{\alpha_A N}{2} \int_0^\infty (e^{\beta\phi} - 1) dx \right]$$

$$= \frac{\alpha_A N}{\tau} \left[\frac{\Delta I}{I_0} - \int_0^\infty (e^{\beta\phi} - 1) dx \right] - \int_0^\infty \frac{2\alpha_A}{\tau} \cosh\beta\phi \rho_T dx . \tag{B19}$$

First, we must express the function

$$g(\Delta I, V_G) = \int_0^\infty (e^{\beta\phi} - 1)dx$$

in terms of the known function

$$f(\Delta I, V_G) = \int_0^\infty (e^{-\beta\phi} - 1)dx = \frac{\Delta I}{I_0}t_i \ .$$

For small $\beta\phi$ we can expand the exponentials, yielding $g = -f$. Furthermore, for large positive $\beta\phi$, $g \gg f$, while large negative $\beta\phi$ requires $g \ll f$. We shall consider the rate of current decay within these limits. Equation (B19) becomes

$$\frac{d}{dt}\left[-\frac{\epsilon_i V_G}{t_i q} - \frac{\Delta I}{I_0}\left[p_0 + \frac{\alpha_A N}{2}\right]t_i + \frac{\alpha_D N}{2}g\right] = \frac{\alpha_A N}{\tau}\left[\frac{\Delta I}{I_0}t_i - g\right] - \int_0^\infty \frac{2\alpha_A}{\tau}\cosh\beta\phi\rho_T dx \ . \tag{B20}$$

The remaining problem is to approximate the last term in Eq. (B20). To do this, we need only consider the conditions under which it becomes important. The current, as we have seen, reflects the magnitude of the screening length which, in turn, directly reflects ρ_T. When ΔI is large, ρ_T is small, and vice versa. Similarly, when ρ_T is large, ϕ is necessarily small for practical values of applied field across the gate insulator. Therefore, the only case in which the last term of Eq. (B20) becomes important is when ρ_T is large and $\beta\phi$ is small. Thus, we can neglect the ϕ dependence, yielding the result

$$\frac{d}{dt}\left[-\frac{\epsilon_i V_G}{t_i q} - \frac{\Delta I}{I_0}\left[p_0 + \frac{\alpha_A N}{2}\right]t_i + \frac{\alpha_D N}{2}g\right] = \frac{\alpha_A N}{\tau}\left[\frac{\Delta I}{I_0}t_i - g\right] - \frac{2\alpha_A}{\tau}\left[-\frac{\epsilon_i V_G}{t_i q} - \frac{\Delta I}{I_0}p_0 t_i\right] \ . \tag{B21}$$

Let us now consider the response to a negative voltage step applied to the gate. For a sufficiently large step, ΔI is initially large and $\beta\phi \ll 0$, so that $f \gg g$. The field effect will then decay via the rate equation

$$\frac{d}{st}\left[-\frac{\epsilon_i V_G}{t_i q} - \frac{\Delta I}{I_0}\left[p_0 + \frac{\alpha_A N}{2}\right]\right]$$

$$= \frac{\alpha_A}{\tau}\left[\frac{\Delta I}{I_0}t_i\right](N + p_0) + \frac{2\alpha_A}{\tau}\left[\frac{\epsilon_i V_G}{t_i q}\right] \ . \tag{B22}$$

At $t = 0$, the left-hand side of Eq. (B6) indicates

$$\Delta I(t = 0) = \frac{I_0}{\left[p_0 + \alpha_A N/2\right]}\frac{\epsilon_i V_G}{t_i q}$$

$$= \left[\frac{\mu_p p_0}{p_0 + \alpha_A N/2}\right]\frac{Z}{L}V_{DS}\frac{\epsilon_i V_G}{t_i} \ .$$

Note the similarity of this expression to the linear case. Since V_G is a constant for $t > 0$, we can eliminate it inside the derivative. If we define

$$I_\infty \equiv \left[\frac{\mu_p p_0}{p_0 + N}\right]\frac{Z}{L}V_{DS}\frac{\epsilon_i}{t_i} \ , \tag{B23}$$

and assume that $\alpha_A N/2 \gg p_0$, then $I_\infty \ll \Delta I$ and Eq. (B22) becomes

$$\frac{d}{dt}(\Delta I) + \frac{2}{\tau}\Delta I = \frac{2}{\tau}I_\infty \simeq 0 \ . \tag{B24}$$

Thus, the field effect initially decays with a time constant of $\tau/2$.

As the current decays, ϕ becomes small and eventually g begins to be comparable to f. For small ΔI,

$$g = -f = -\frac{\Delta I}{I_0}t_i \ ,$$

and Eq. (B21) becomes

$$\frac{d}{dt}\left[-\frac{\Delta I}{I_0}\left[p_0 + \frac{\alpha_A N}{2} + \frac{\alpha_D N}{2}\right]\right]$$

$$= \frac{\alpha_A}{\tau}\left[\frac{\Delta I}{I_0}t_i\right](2N + p_0) + \frac{2\alpha_A}{\tau}\left[-\frac{\epsilon_i V_G}{t_i q}\right]$$

or

$$\frac{d}{dt}\Delta I + \left[\frac{4\alpha_A}{(\alpha_A + \alpha_D)\tau}\right]I = \frac{4\alpha_A}{(\alpha_A + \alpha_D)\tau}I_\infty \simeq 0 \ . \tag{B25}$$

Thus, for very large times and small currents, the rate of decay is $(\tau/2)[(\alpha_A + \alpha_D)/2\alpha_A]$. Note that this is the same result obtained from the linear analysis.

*Current Address: Bell Laboratories, Murray Hill, N.J.

[1]P. W. Anderson, Phys. Rev. Lett. 34, 953 (1975).

[2]R. A. Street and N. F. Mott, Phys. Rev. Lett. 35, 1293 (1975).

[3]N. F. Mott, E. A. Davis, and R. A. Street, Philos. Mag. 32, 961 (1975).

[4]M. Kastner, D. Adler, and H. Fritzsche, Phys. Rev. Lett. 37, 1504 (1976).

[5]D. Adler, J. Non-Cryst. Solids 35/36, 819 (1980).

[6]D. Adler and E. J. Yoffa, Phys. Rev. Lett. 36, 1197 (1976); Can. J. Chem. 55, 1920 (1977).

[7]H. Fritzsche and S. R. Ovshinsky, J. Non-Cryst. Solids 2, 393 (1970).

[8]R. F. Egerton, Appl. Phys. Lett. 19, 203 (1971).

[9]A. W. Levy, M. Green, and W. Gee, J. Phys. C 7, 352 (1974).

[10]P. A. Tick and J. H. P. Watson, J. Non-Cryst. Solids 13, 229 (1973).

[11]J. M. Marshall and A. E. Owen, Philos. Mag. 33, 457 (1976).

[12]J. E. Mahan and R. H. Bube, J. Non-Cryst. Solids 24, 29 (1977).

[13]N. A. Radjy and M. Green, Philos. Mag. 41, 497 (1980).

[14]D. Adler, in Amorphous and Liquid Semiconductors, edited by W. E. Spear (Centre for Industrial Consultancy and Liaison, Edinburgh, 1977), p. 695.

[15]H. Fritzsche, in Amorphous and Liquid Semiconductors, edited by W. E. Spear (Centre for Industrial Consultancy and Liaison, Edinburgh, 1977), p. 3.

[16]D. Adler, Sol. Cells 2, 199 (1980).

[17]M. Kastner and H. Fritzsche, Philos. Mag. B37, 199 (1978).

[18]R. N. Hall, Phys. Rev. 87, 387 (1952).

[19]W. Shockley and W. T. Read, Phys. Rev. 87, 835 (1952).

[20]A. Rose, Concepts in Photoconductivity and Allied Problems (Interscience, New York, 1963), p. 118.

[21]S. G. Bishop, U. Strom, and P. C. Taylor, Phys. Rev. Lett. 36, 543 (1976).

[22]D. Adler, M. S. Shur, M. Silver, and S. R. Ovshinsky, J. Appl. Phys. 51, 3289 (1980).